Crystallization Regulation by Introducing Multistage Growth Template Enables Efficient and Stable Inverted Perovskite Solar Cells

Jiaqi Zhang[a], Runying Dai[a], Jia Yang*[a], Yikun Liu[b], Jianxin Yu[a], Licheng Tan*[b], Yiwang Chen*[ab]

J. Zhang, R. Dai, J. Yang, J. Yu, Prof. Y. Chen

[a.]Key Lab of Fluorine and Silicon for Energy Materials and Chemistry of Ministry of Education/ College

of Chemistry and Materials, Jiangxi Normal University, 99 Ziyang Avenue, Nanchang 330022, China

Y. Liu, Prof. L. Tan, Prof. Y. Chen

[b.]College of Chemistry and Chemical Engineering/ Institute of Polymers and Energy Chemistry (IPEC)/

 Film Energy Chemistry for Jiangxi Provincial Key Laboratory (FEC), Nanchang University, 999 Xuefu

Avenue, Nanchang 330031, China

Email: ywchen@ncu.edu.cn (Y. C.); yangjia@jxnu.edu.cn (J. Y.); tanlicheng@ncu.edu.cn (L. T.).

Experimental Section

Original NiO$_x$ and NiO$_x$-ILs NPs synthesis: For the H-NiO$_x$ NPs, first, 14.54g Ni(NO$_3$)$_2$·6H$_2$O (Sigma-Aldrich, 99.999%) was dissolved in 100 mL distilled water. At the same time, 1-Hexyl-3-methylimidazolium tetrafluoroborate ([C$_6$MIM]BF$_4$, 200mg, TCI, 98%) was dissolved in 20 mL deionized water and magnetically stirred for 10 min. Then, 2 mL [C$_6$MIM]BF$_4$ solution added slowly into the Ni(NO$_3$)$_2$·6H$_2$O solution and stirred for 20 min at 80 °C. Subsequently, 0.4 g/mL NaOH solution was added dropwise to the solution until the pH value reached 10. The obtained green emulsion was centrifuged after stirring for 20 min, and the precipitate was washed three times with deionized water. Obtained products was vacuum dried for 48 hours. Finally, the obtained green solid small pieces were pulverized and calcined at 270 °C for 2 h to synthesize a dark black powder as the final product. Other NiO$_x$-ILs NPs (1-Ethyl-3-methylimidazolium tetrafluoroborate [C$_2$MIM]BF$_4$ or 1-Decyl-3-methylimidazolium tetrafluoroborate [C$_{10}$MIM]BF$_4$) were obtained by the same method. The original NiO$_x$ NPs were obtained by following the synthesized process in previous report.[1] Afterwards, original NiO$_x$ and NiO$_x$-ILs NPs were dispersed in deionized water by ultrasonication to prepare corresponding solutions.

Materials:

All chemicals were used directly without any treatment after purchase. Chlorobenzene (CB, anhydrous, 99.8%), N, N-dimethylformamide (DMF, anhydrous, 99.8%), bathocuproine (BCP, 96.0%), [4-(3,6-dime-thyl-9H-carbazol-9yl) butyl] phosphonic acid (Me-4PACz), isopropanol (IPA) and dimethyl sulfoxide (DMSO, anhydrous, ≥99.9%) were purchased from Sigma-Aldrich. [6, 6]-Phenyl-C61-butyric acid methyl ester (PC$_{61}$BM) and lead iodide (PbI$_2$, 99.999%) precursor were obtained from Alfa Aesar. (1,3-Diaminopropane Dihydroiodide) PDAI was purchased from Innochem.

Preparation of original NiO$_x$ and NiO$_x$-ILs HTLs: The patterned indium tin oxide (ITO) glass substrate was cleaned sequentially in dichloromethane, deionized water, and isopropyl alcohol for 20 min by

ultrasonic processing, then blown dried with flowing nitrogen. Subsequently, treated by air plasma for 10 min. Afterwards, the original NiO_x and NiO_x-ILs solution (20mg/ml in H_2O) was spin-coated on ITO with 2000 rpm for 30 s and annealed in air at 120 °C for 30 min. After cooling down, the substrate was moved to glove box filled with N_2.

CsFAMA mixed perovskite films: The mixed-cation perovskite $Cs_{0.05}(FA_{0.92}MA_{0.08})_{0.95}Pb(I_{0.92}Br_{0.08})_3$ was prepared by mixing PbI_2 (645.4 mg), FAI (170.9 mg), $MABr_2$ (11.9 mg), $FABr_2$ (28.7 mg), CsI (18.2 mg) powder in DMF/DMSO (4:1, v/v) with stirred over night at 60 °C. The mixed-cation perovskite films were obtained by a two-step spin-coating process with 1000 rpm for 10 s and 4000 rpm for 30 s. 200 μL chlorobenzene was dropped at the 20 s of the second spin-coating step on spinning substrate. Lastly, the substrate was annealed at 100 °C for 30 min.

Electron transport layer and electrode: The $PC_{61}BM$ solution (20 mg mL^{-1} in anhydrous CB) was spin-coated on the top of perovskite with 2000 rpm for 30 s, then annealed at 100 °C for 10 min. Subsequently, the BCP (0.5 mg mL^{-1} in anhydrous ethanol) was spin-coated with 4500 rpm for 30 s on $PC_{61}BM$ film. Ultimately, the Ag anode above 100 nm was deposited on the BCP at vacuum environment.

Fabrication of champion perovskite solar cell based on NiO_x-ILs/Me-4PACz: NiO_x-ILs NPs was dispersed in deionized water to form NiO_x-ILs ink (10 mg ml^{-1}). The as-prepared NiO_x-ILs ink was spin-coated on the ITO substrate at 2000 rpm for 30s, then annealing at 150 °C for 30 min in air. Subsequently, the solution of Me-4PACz with a concentration of 1 mmol L^{-1} in absolute ethanol was spin-coated on NiO_x film at 3000 rpm for 20 s, followed by annealing at 100 °C for 10 min. For perovskite precursor preparation, 1.5 M perovskite precursor solution was prepared by mixing 19.5 mg of CsI, 219.3 mg of FAI, 23.8 mg of MAI and 760.7 mg of PbI_2 (10% of excess) in 1 ml DMF/DMSO (4:1, v/v) mixed solvent with a chemical formula of $Cs_{0.05}FA_{0.85}MA_{0.1}PbI_3$. The perovskite precursor was spin-coated on substrates at 1000 rpm for

10 s, subsequently at 5000 rpm for 40 s, then 170 µL CB was dripped onto the center of film at 15 s before the end of spin-coating process. The substrates were immediately transferred to the hotplate and annealed at 100 °C for 20 min. For the interfacial passivation layer, PDAI with the concentration of 1 mg mL^{-1} in IPA was spin-coated on top of perovskite films (5000 rpm, 30 s) and annealed at 100 °C for 5 min. Subsequently, rinse with 120 µL IPA (5000 rpm, 30 s). Finally, 20 nm C$_{60}$ at a rate of 0.5 Å s^{-1}, 5 nm BCP at a rate of 0.5 Å s^{-1} and 100 nm silver electrode at a rate of 1.0 Å s^{-1} were thermally evaporated, respectively, under high vacuum (< 4×10^{-6} Torr).

Device characterization: The X-ray photoelectron spectroscopy (XPS) measurement was measured by a Thermo-VG scientific ESCALAB 250 photoelectron spectrometers with a monochromatic Al (Kα) (1,486.6 eV) X-ray source. Scanning electron microscopy (SEM) measurement and energy-dispersive X-ray spectrometry (EDS) mapping images were examined using SU8020 SEM with a voltage of 8 kV. Atomic force microscopy (AFM) images were performed by MultiMode 8-HR (Bruker) atomic force microscope. A Rigaku D/Max-B X-ray diffractometer with Bragg-Brentano parafocusing geometry was applied to test X-ray diffraction (XRD) patterns. The ultraviolet-visible (UV-Vis) spectra was recorded on a SHIMADZU, UV-2600 spectrophotometer in 300-900 nm wavelength range. The steady-state photoluminescence (PL) and time-resolved photoluminescence (TRPL) spectra were performed by an Edinburgh instruments FLS920 spectrometer (Edinburgh Instruments Ltd.). Current density-voltage (J-V) characteristics of PVSCs were measured using a source meter (Keithley 2400), equipped with a light source (100 mW/cm^2) under AM 1.5 G filter. The reverse scan range is from 1.2 V to 0 V, with 20 mV for each step. External quantum efficiency (EQE) were characterized under monochromatic illumination (Oriel Cornerstone 260 1/4 m monochromator equipped with an Oriel 70613NS QTH lamp), and the measurement scope was 300–900 nm. Electrical impedance spectroscopy (EIS) of the PVSCs was measured in a frequency range from 1 MHz to 10 mHz by using Zahner electrochemical workstation at an applied bias

equivalent to the open-circuit voltage of the cell under 1 sun illumination. The hole mobilities were deduced from a space-charge limited current (SCLC) model utilizing the Mott Gurney law.

First-principles calculations: All the first-principles density functional theory (DFT) calculations are carried out under the generalized gradient approximation (GGA) condition by using the Perdew-Burke-Ernzerhof (PBE) formulation.[2-4] We have chosen the projected augmented wave (PAW) potentials to describe the ionic cores and take valence electrons into account which using a plane wave basis set with a kinetic energy cutoff of 520 eV.[5,6] The Gaussian smearing method with a width of 0.05 eV was used to allow partial occupancies of the Kohn-Sham orbital. While the energy change is less than 10^{-4} eV, the electronic energy are considered self-consisten. Meanwhile, a geometry optimization is considered convergent when the energy change is less than 0.05 eV $Å^{-1}$. In addition, the surface vacuum spacing in the direction perpendicular to the plane of the structure is 20 Å. The Brillouin zone integration is performed using 2×2×1 Monkhorst-Pack k-point sampling structure. Finally, the adsorption energies (E_{ads}) can be calculated as $E_{ads} = E_{ad/sub} - E_{ad} - E_{sub}$, where $E_{ad/sub}$, E_{ad}, and E_{sub} are the total energies of the optimized adsorbate/substrate system, the adsorbate in the structure, and the clean substrate, respectively.
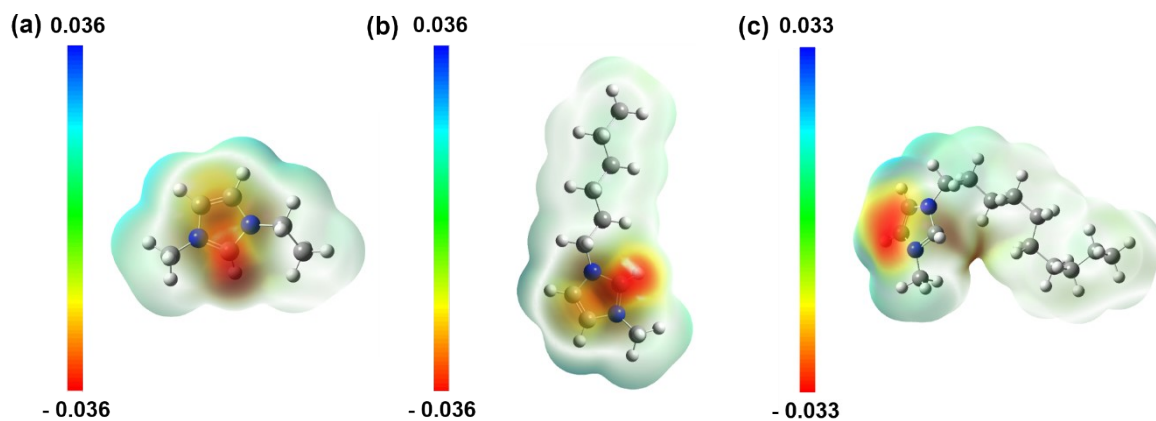
Figure S1. Calculated electrostatic potential (ESP) profile of (a) [C_2MIM]BF$_4$, (b) [C_6MIM]BF$_4$ and (c) [C_{10}MIM]BF$_4$. A six-electron conjugated large π-bond exists on the imidazole ring, where the C(2) atom between the two N atoms has a relatively low electron cloud density. Therfore, the hydrogen atom attaching to C(2) possess a strong ability to accept electrons, which is more conducive to the formation of hydrogen bonds with NiO$_x$.
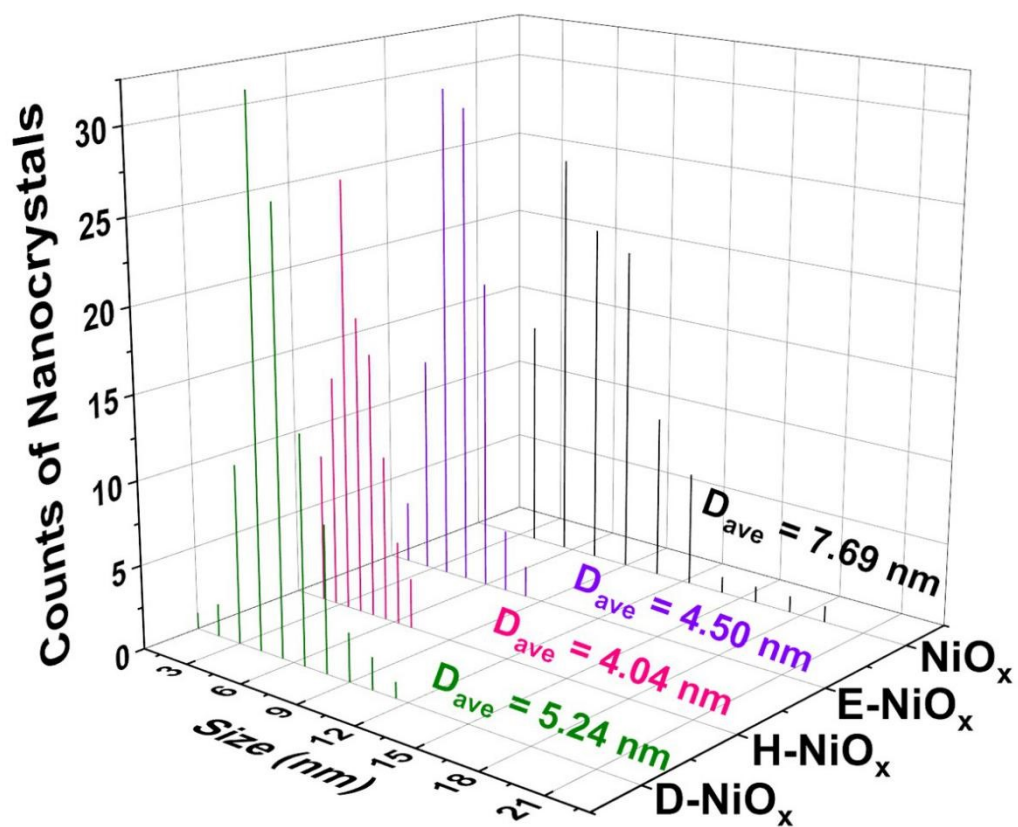
Figure S2. The histogram of particle sizes for NiO_x, $E\text{-}NiO_x$, $H\text{-}NiO_x$ and $D\text{-}NiO_x$.
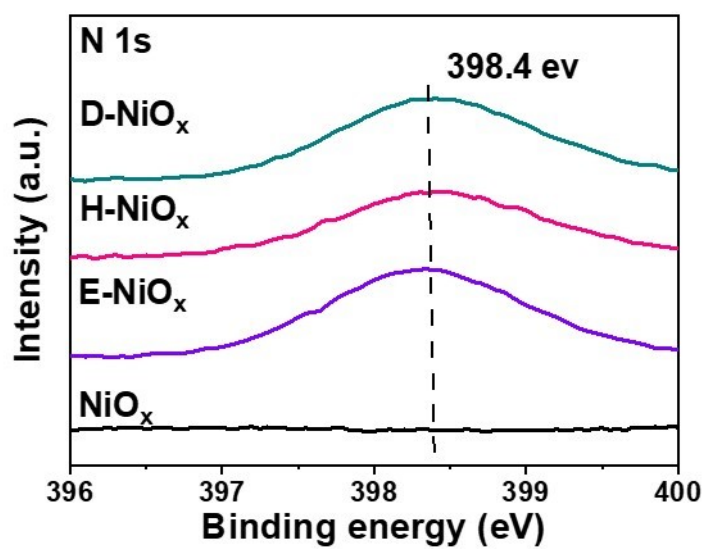
Figure S3. XPS spectra of N 1s for NiO_x, $E-NiO_x$, $H-NiO_x$ and $D-NiO_x$.
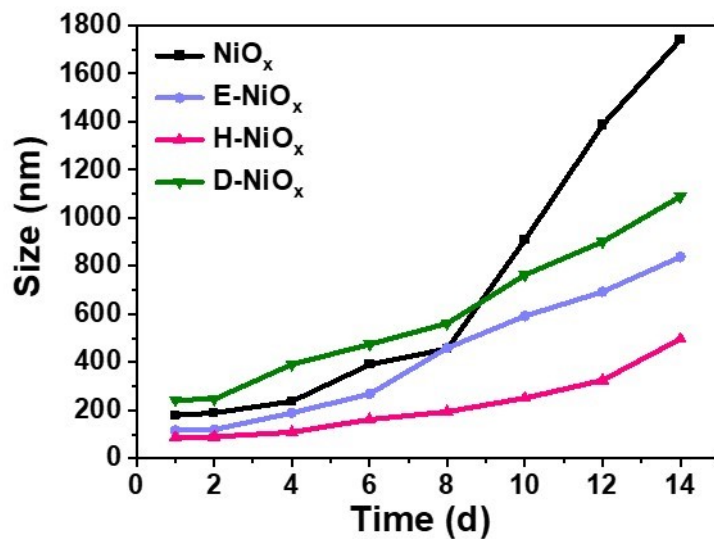
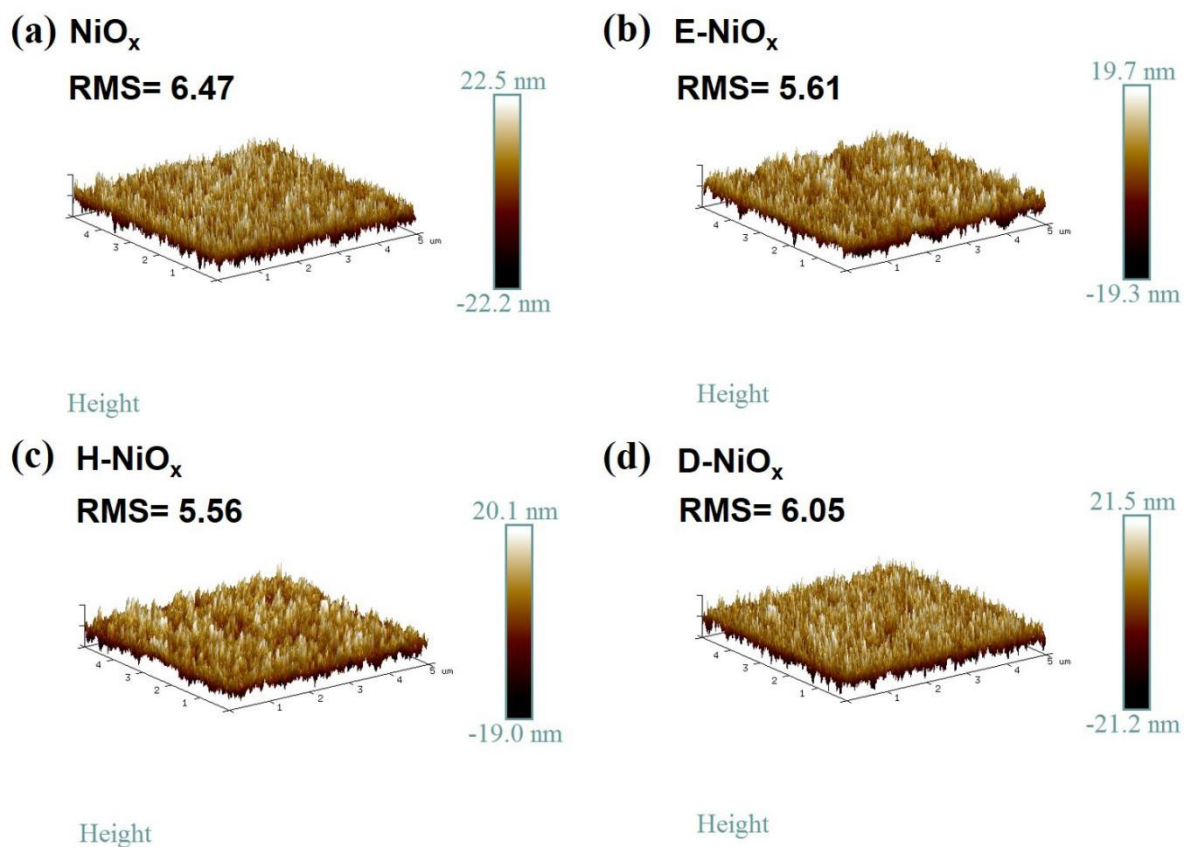**Figure S4.** Size distribution of different NiO_x NPs as a function of time upon standing

(a) NiO$_x$
RMS= 6.47

22.5 nm

-22.2 nm

Height

(b) E-NiO$_x$
RMS= 5.61

19.7 nm

-19.3 nm

Height

(c) H-NiO$_x$
RMS= 5.56

20.1 nm

-19.0 nm

Height

(d) D-NiO$_x$
RMS= 6.05

21.5 nm

-21.2 nm

Height

Figure S5. AFM images of (a) NiO$_x$, (b) E-NiO$_x$, (c) H-NiO$_x$ and (d) D-NiO$_x$.
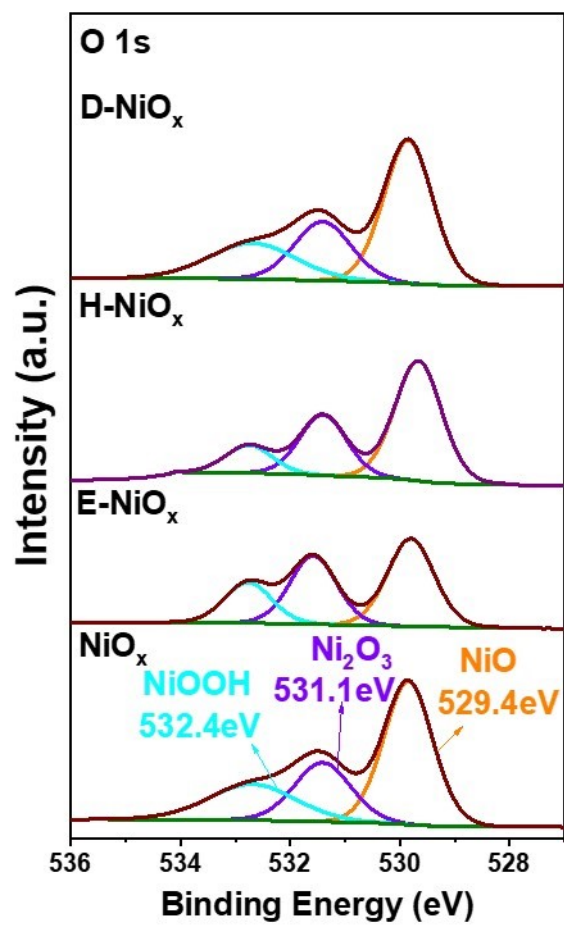
Figure S6. XPS spectra of O 1s for NiO_x, $E-NiO_x$, $H-NiO_x$ and $D-NiO_x$ films.

(a) NiOx SP= 4.67 mV   16.2 mV / -18.8 mV   Potential   1.0 µm

(b) E-NiOx SP= 5.37 mV   18.6 mV / -25.3 mV   Potential   1.0 µm

(c) H-NiOx SP= 10.6 mV   36.9 mV / -43.3 mV   Potential   1.0 µm

(d) D-NiOx SP= 5.27 mV   18.6 mV / -20.9 mV   Potential   1.0 µm
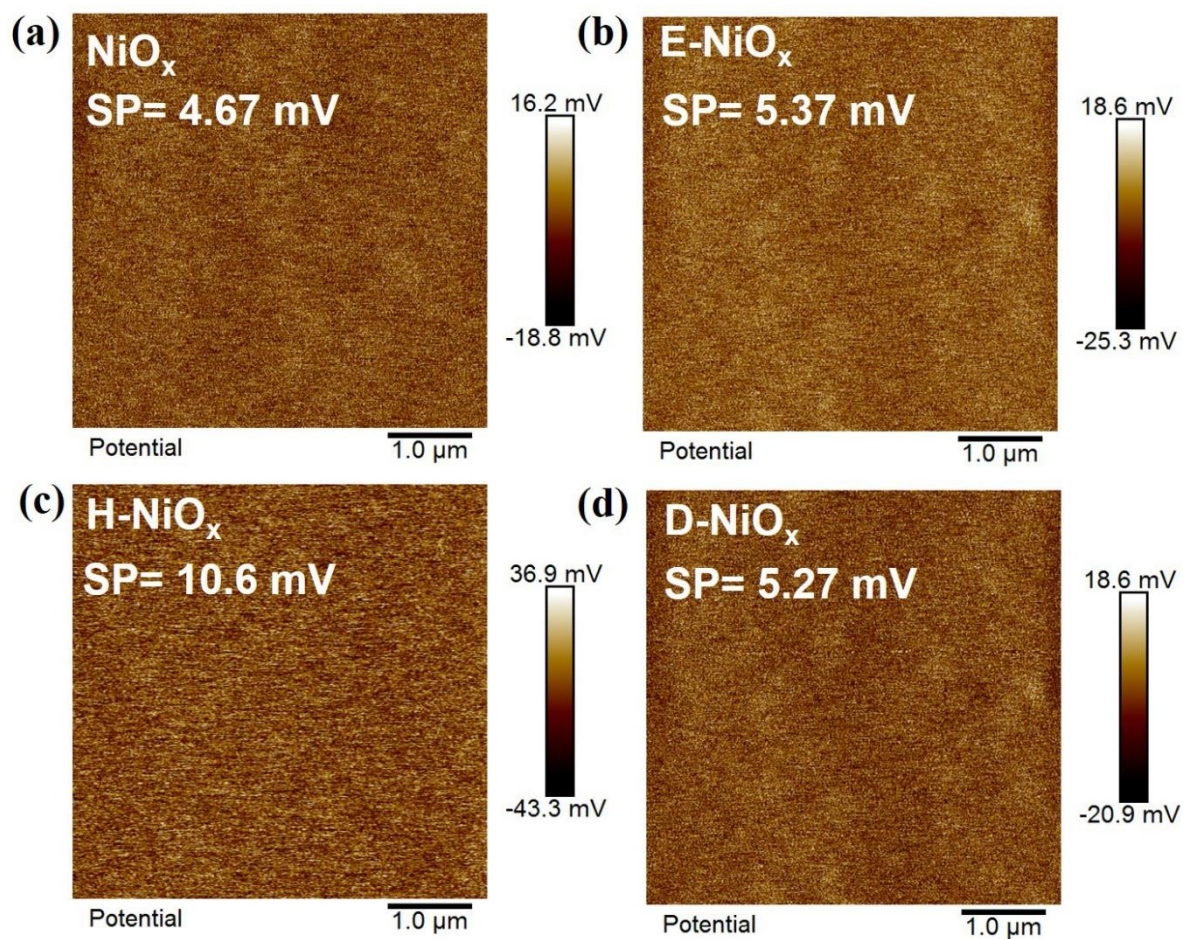
Figure S7. KPFM images of (a) NiO_x, (b) E-NiO_x, (c) H-NiO_x and (d) D-NiO_x.
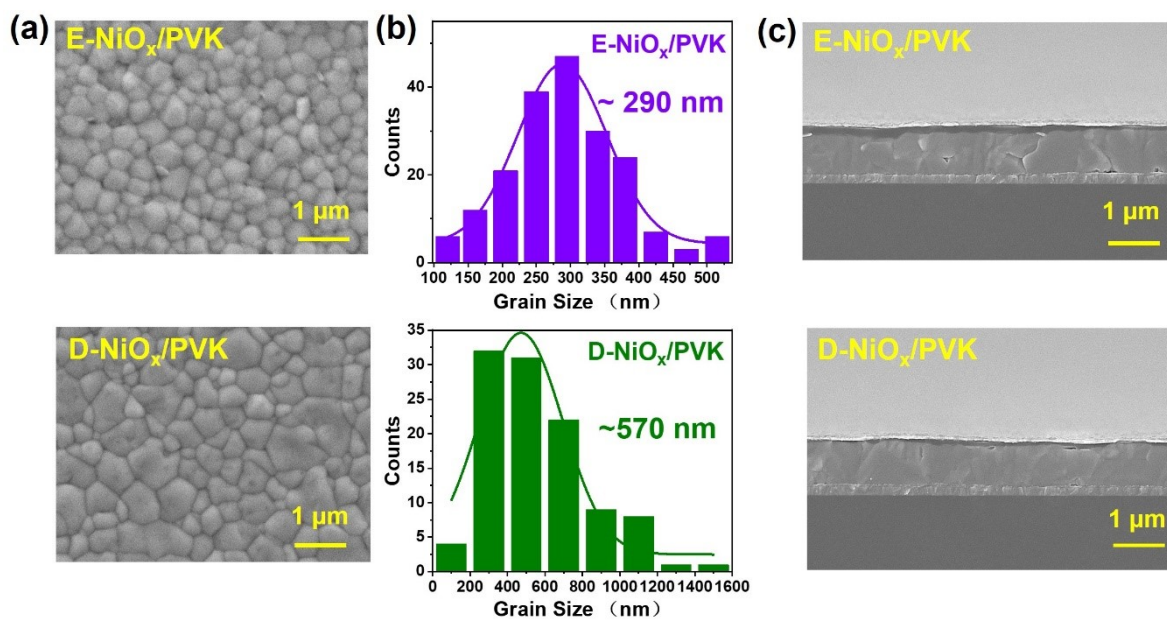
Figure S8. (a) SEM images, (b) Grain size statistics of perovskite films and (c) Cross-sectional SEM images of PVSCs based on E-NiO$_x$ and D-NiO$_x$.
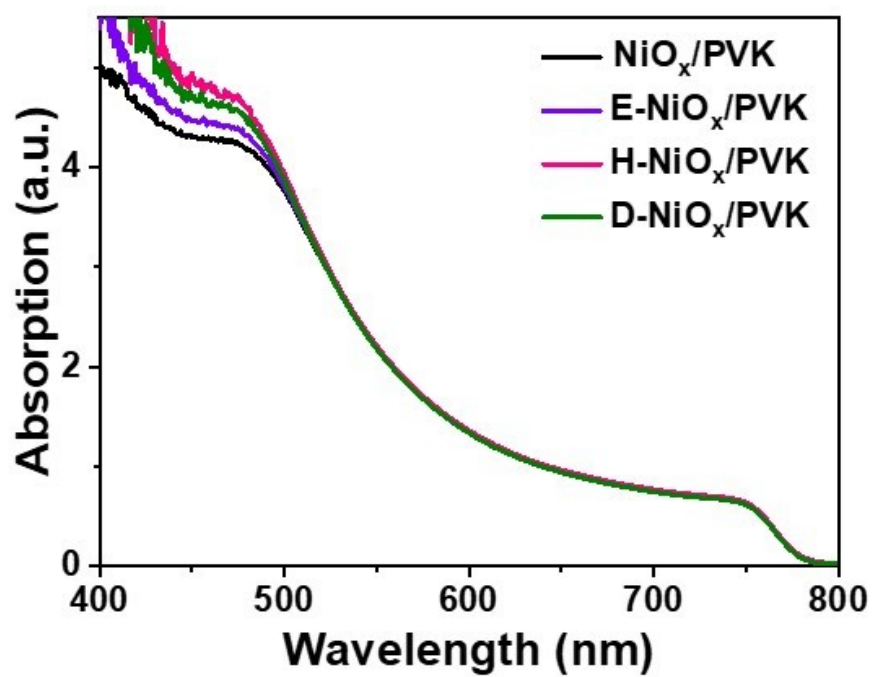
Figure S9. UV-Vis absorption spectra of perovskite films deposited on different HTLs (NiO_x, E-NiO_x, H-NiO_x, D-NiO_x).
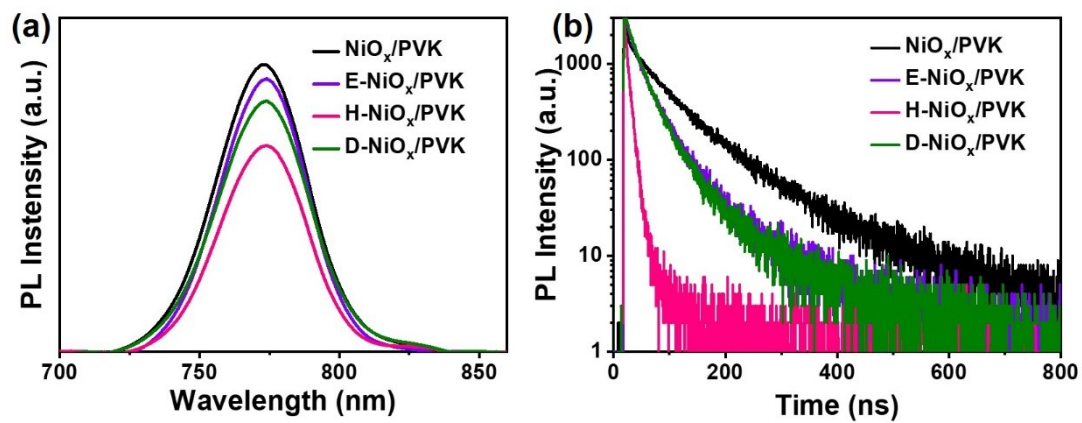
Figure S10. (a) Steady-state PL spectra and (b) TRPL spectra of perovskite films deposited on NiO_x, E-NiO_x, H-NiO_x and D-NiO_x, respectively.
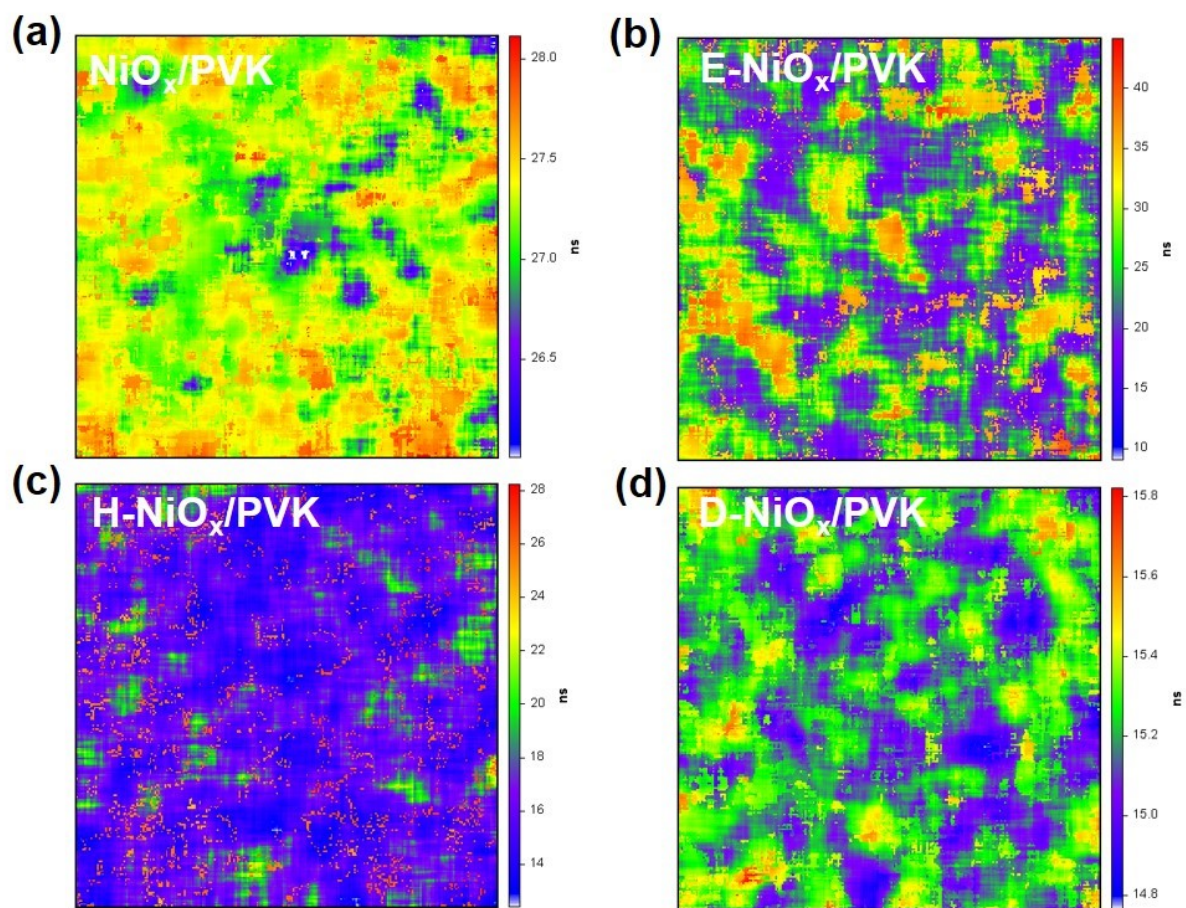
Figure S11. PL lifetime images of perovskite films based on (a) NiO_x, (b) E-NiO_x, (c) H-NiO_x and (d) D-NiO_x, respectively.
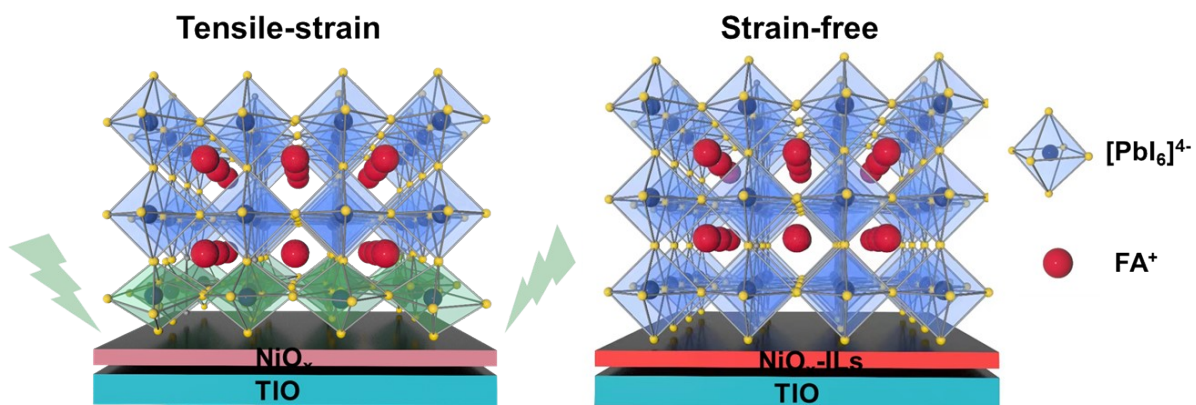
Figure S12. Schematic diagrams of lattice strain distribution in perovskite grains deposited on NiO$_x$ and H-NiO$_x$ substrates.
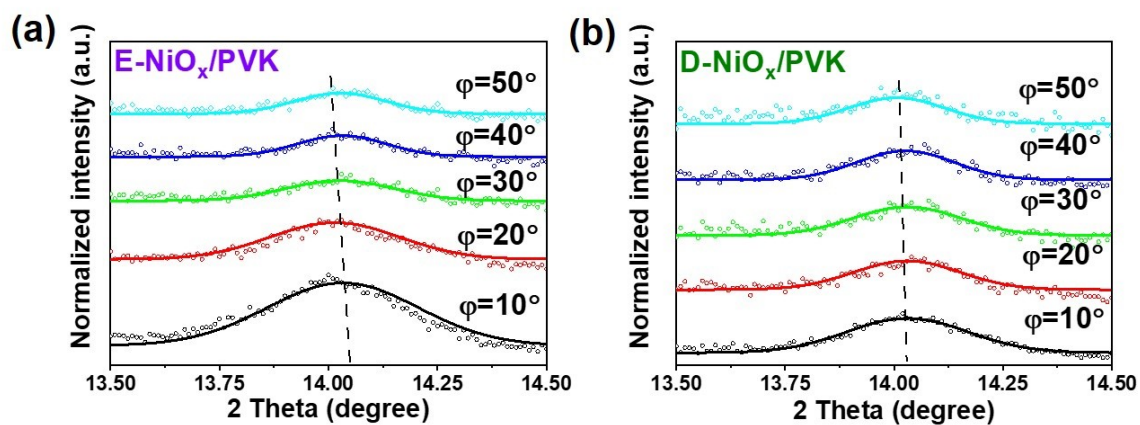
Figure S13. GIXRD patterns of perovskite films deposited on (a) E-NiO$_x$ and (b) D-NiO$_x$ at different tilt angles.
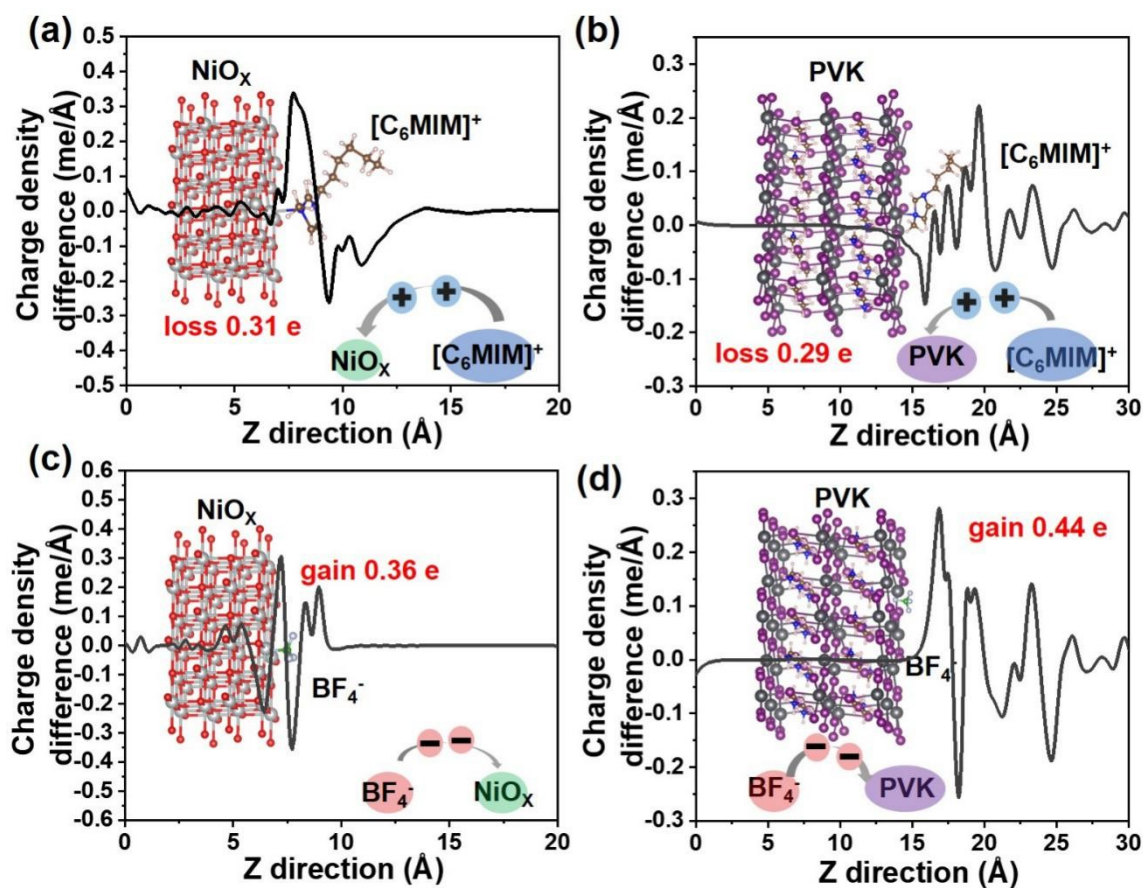
Figure S14. Charge density difference of (a) $[C_6MIM]^+/NiO_x$, (b) $[C_6MIM]^+/perovskite$, (c) BF_4^-/NiO_x and (d) $BF_4^-/perovskite$. The NiO_x layer with $[C_6MIM]^+$ adsorption loses 0.31 e more than that of the perovskite with $[C_6MIM]^+$ adsorption, which results in the nickel ion of NiO_x becomes more positive, there by increasing the Ni^{3+} concentration. Furthermore, the BF_4^- adsorbs on perovskite layer loses 0.44 e, more than that adsorps on NiO_x, implying more strong interaction between BF_4^- and perovskite.
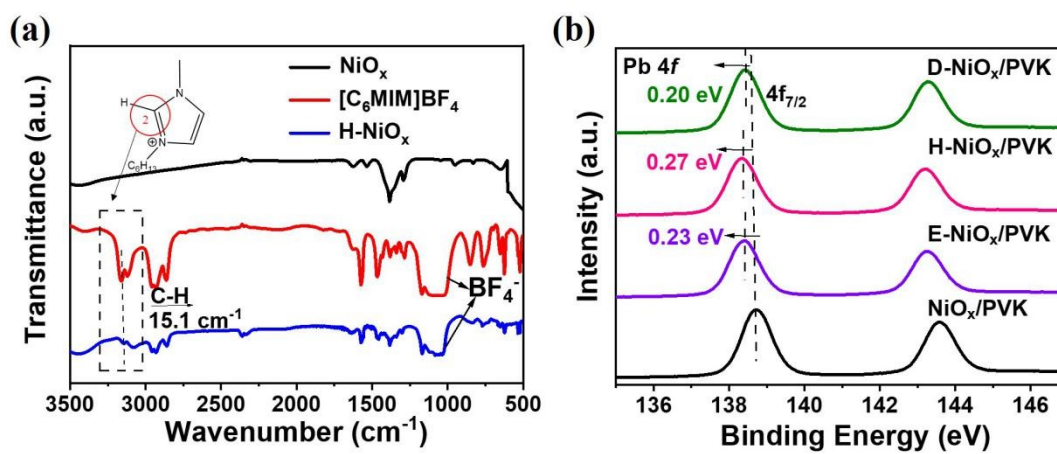
19

Figure S15. (a) FTIR spectra of NiO_x, $[C_6MIM]BF_4$ and $H\text{-}NiO_x$, respectively. (b) XPS spectra of Pb 4f for the perovskite films based on NiO_x, $E\text{-}NiO_x$, $H\text{-}NiO_x$ and $D\text{-}NiO_x$, respectively.
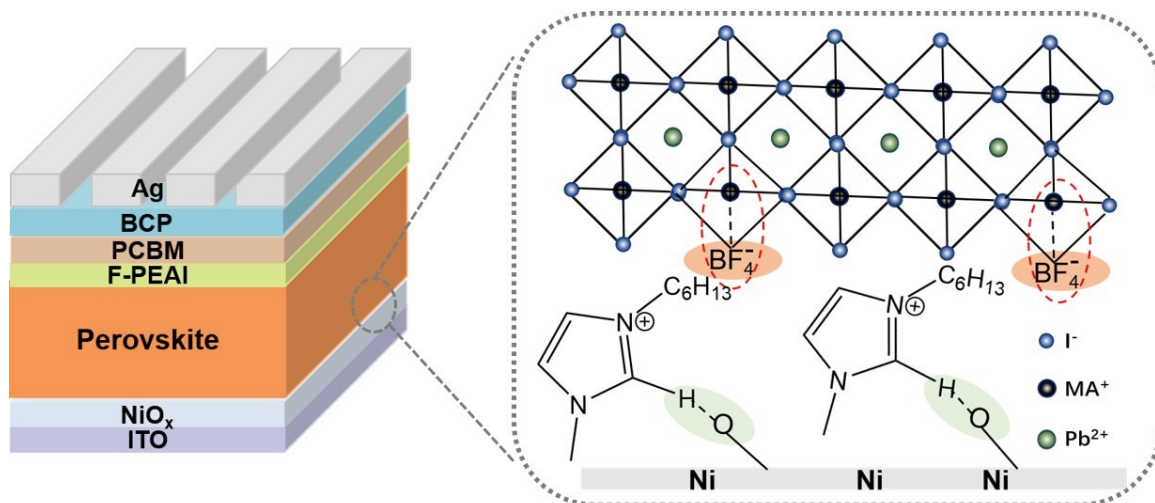
Figure S16. Schematic diagram of PVSCs based on H-NiO$_x$, where the BF$_4^-$ of [C$_6$MIM]BF$_4$ can fill I$^-$ vacancies to directly serve as the structural component of perovskite crystals and the [C$_6$MIM]$^+$ can passivated the surface defects of NiO$_x$.
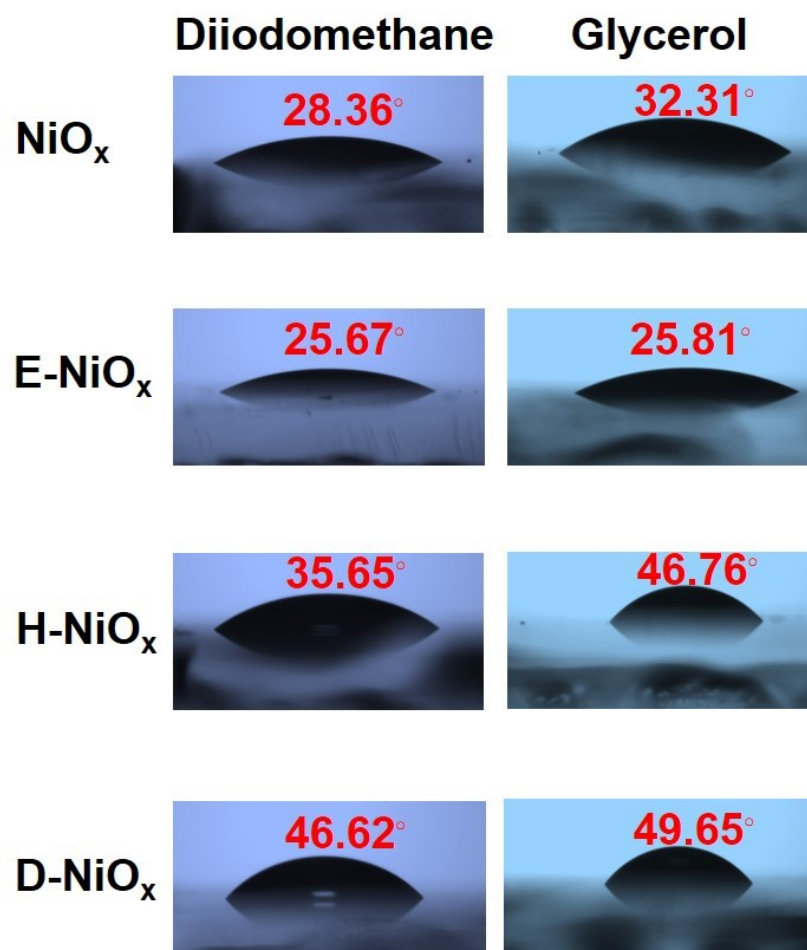
Figure S17. The contact angle measurements of diiodomethane and glycerol on different NiO_x.
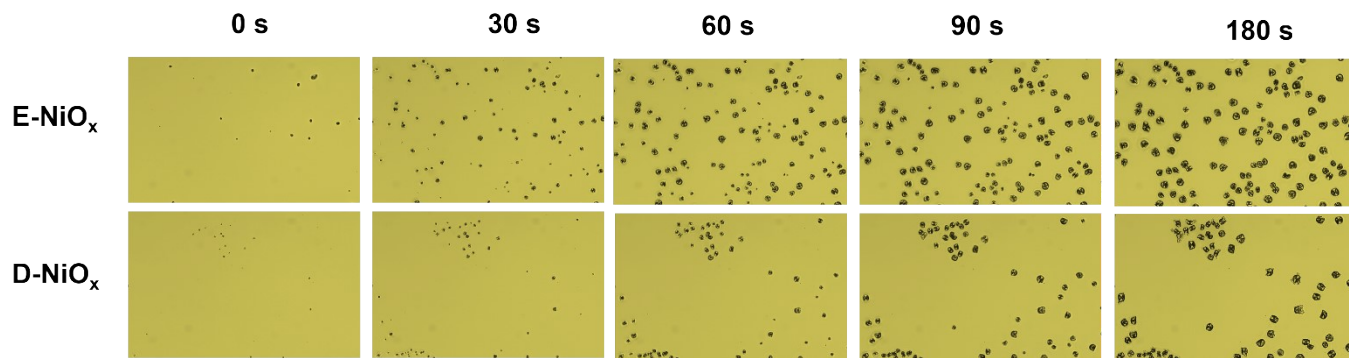
| | 0 s | 30 s | 60 s | 90 s | 180 s |

Figure S18. In-situ microscopy photographs of the evolutions of perovskite precursor as a function of time of perovskite precursor based on E-NiO$_x$ and D-NiO$_x$ film.
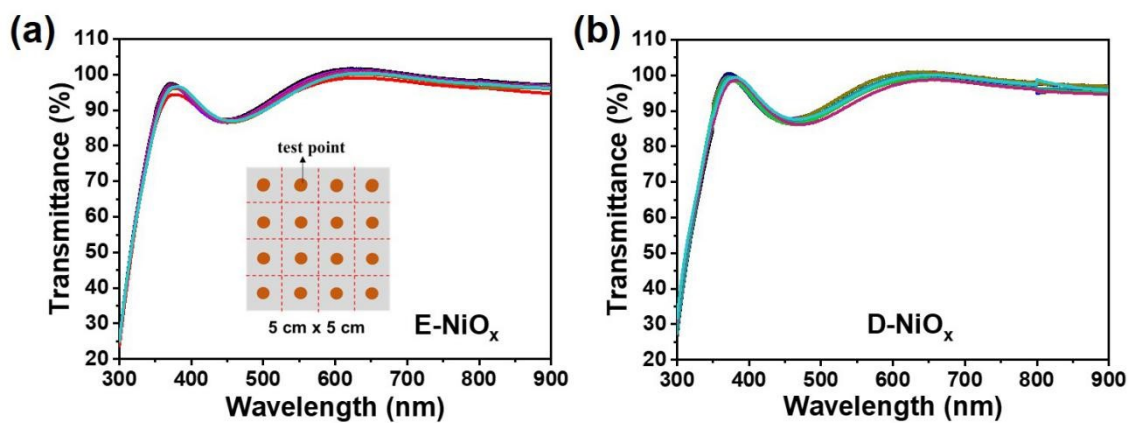
Figure S19. Optical transmission spectra of (a) E-NiO$_x$ and (b) D-NiO$_x$ films on 5 cm x 5 cm substrates**.**
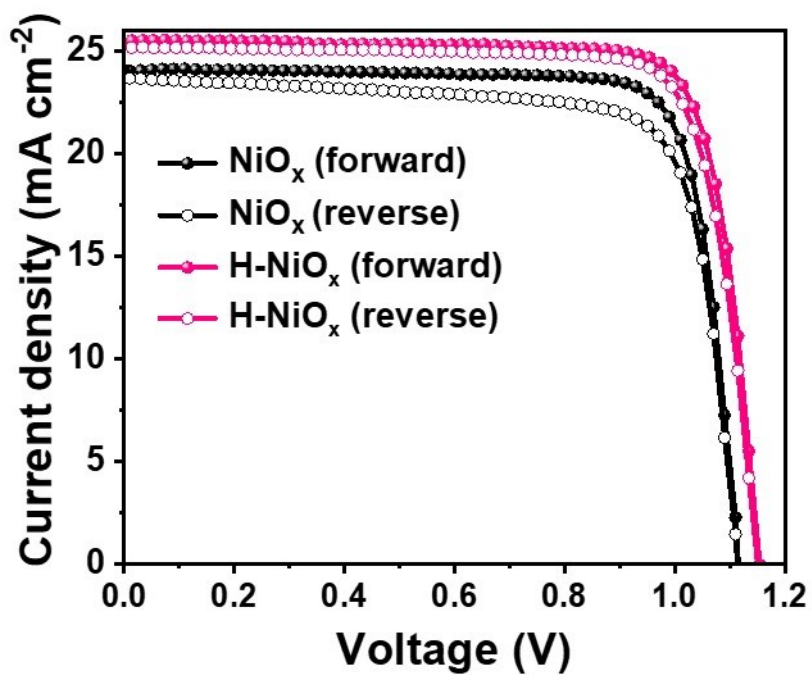
Figure S20. *J-V* curves measured in both forward and reverse scan directions under AM 1.5 G illumination (100 mW·cm^{-2}) for PVSCs with HTL of NiO$_x$ and H-NiO$_x$, respectively.
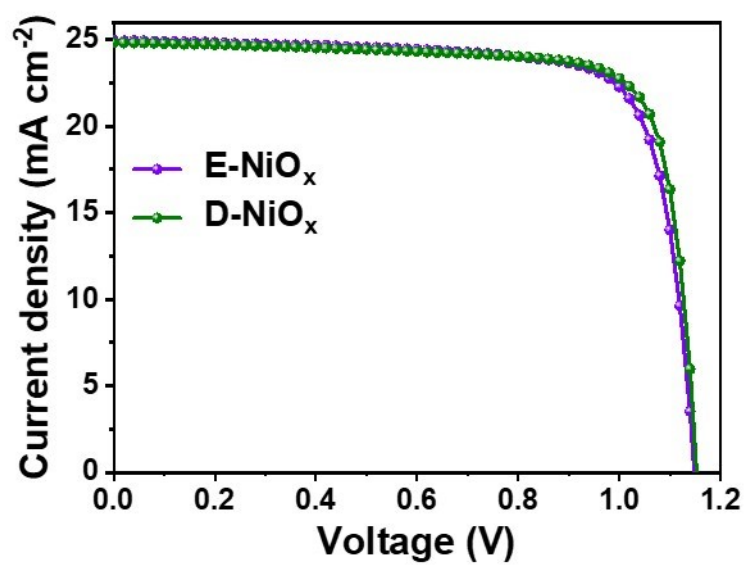
Figure S21. *J-V* curves of the champion devices based on different HTLs (E-NiO$_x$, D-NiO$_x$) measured under standard AM 1.5 G illumination (100 mW cm^{-2}).
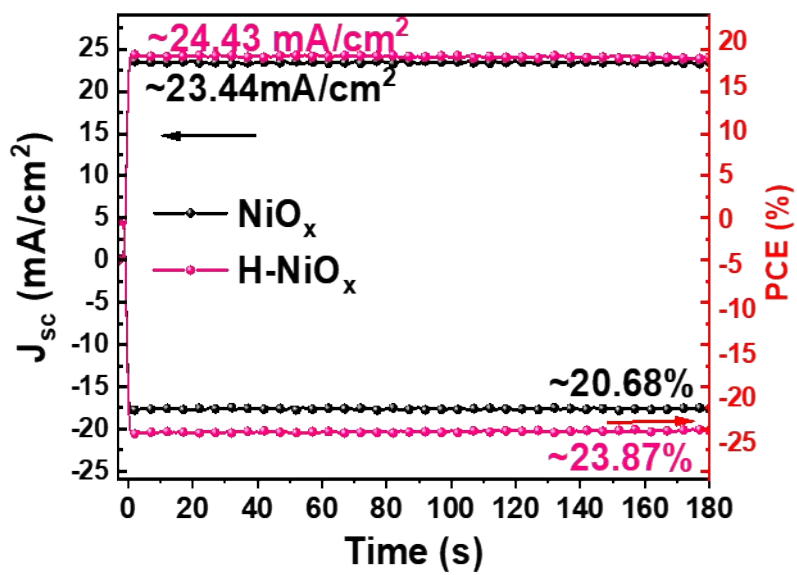
Figure S22. The steady-state photocurrent and output PCE at the maximum power point of the devices based on NiO_x and $H-NiO_x$ HTLs.
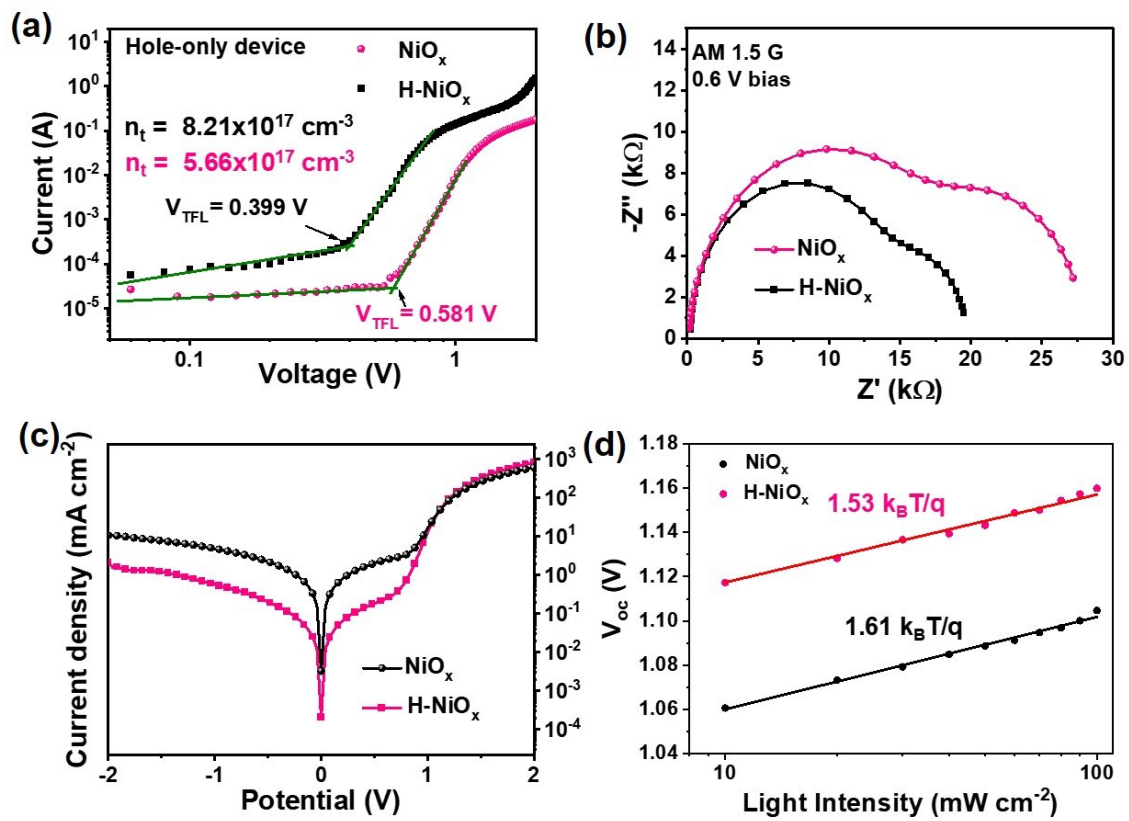
Figure S23. (a) Dark *J-V* curves under SCLC model based on the device structure of ITO/NiO$_x$ or H-NiO$_x$/perovskite/Au. (b) *V*$_{oc}$ versus light intensity, (c) Nyquist plots, and (d) dark *J-V* curves of the corresponding devices.

Table S1. Near-surface atomic ratios of different NiO_x films.

HTLs	Ni^{3+} (eV)	Ratio (%)	Ni^{2+} (eV)	Ratio (%)	Ni^{3+}/Ni^{2+} (%)
NiO_x	855.6	41.54	853.8	14.61	2.843
$E\text{-}NiO_x$	855.7	43.76	854.0	13.47	3.248
$H\text{-}NiO$	855.9	44.02	854.1	12.75	3.453
$D\text{-}NiO_x$	855.7	41.98	854.0	14.20	2.956

Table S2. Contact angle and surface energy data of NiO_x, $E\text{-}NiO_x$, $H\text{-}NiO_x$ and $D\text{-}NiO_x$.

Samples	Contact angle (degree)		Surface energy (mJ/m^2)		
	diiodomethane	glycerol	disperse	polar	tolal
NiO_x	28.36	32.31	44.89	11.92	56.81
$E\text{-}NiO_x$	25.67	25.81	45.91	13.71	59.62
$H\text{-}NiO_x$	35.65	46.76	41.72	7.560	49.28
$D\text{-}NiO_x$	46.62	49.65	36.13	9.260	45.39

Table S3. *J-V* parameters of PVSCs based on different HTLs measured in both forward and reverse scan directions under AM 1.5 G illumination (100 mW·cm^{-2}).

HTLs	Scan direction	V_{oc} (V)	J_{sc} (mA·cm^{-2})	FF (%)	PCE (%)	HI (%)
NiO$_x$	Forward	1.115	24.04	81.43	21.83	0.071
	Reverse	1.113	23.69	76.89	20.28	
H-NiO$_x$	Forward	1.161	25.32	81.46	23.96	0.013
	Reverse	1.157	25.19	81.06	23.66	

Table S4. The reported efficiency of representative NiO_x-based PVSCs.

HTL type	Architecture [#]	PCE (%)		Year	Ref. *
		0.04 cm^2	1.01 cm^2		
Single HTL	ITO/NiO_x/$Cs_{0.05}(MA_{0.15}FA_{0.85})_{0.95}Pb(I_{0.85}Br_{0.15})_3$/PCBM+$C_{60}$/BCP/Cr/Au	22.62	20.19	2022	[7]
	ITO/NiO_x/$Cs_{0.05}FA_{0.85}MA_{0.1}PbI_3$/PCBM/BCP/Ag	23.91	NO	2022	[9]
	ITO/NiO_x/$Cs_{0.05}(MA_{0.05}FA_{0.95})_{0.95}Pb(I_{0.95}Br_{0.05})_3$/BzMIMBr/$C_{60}$/BCP/Cu	23.61	18.97% (16 cm^2)	2023	[48]
	ITO/NiO_x/$Cs_{0.05}(FA_{0.92}MA_{0.08})_{0.95}Pb(I_{0.92}Br_{0.08})_3$/F-PEAI/PCBM/BCP/Ag	**24.69**	**21.23**	**This work**	
Multiple HTLs	ITO/NiO_x/PTAA/$Cs_{0.05}(FA_{0.83}MA_{0.17})_{0.95}Pb(I_{0.83}Br_{0.17})_3$/PCBM/BCP/Ag	21.75	NO	2022	[12]
	ITO/NiO_x/PTAA/$FA_{0.95}Cs_{0.05}PbI_3$/PCBM/BCP/Ag	23.49	NO		
	ITO/NiO_x/PTAA/Al_2O_3/$Cs_{0.05}FA_{0.95}PbI_3$/PCBM/BCP/Ag	25.12	22.48	2023	[49]
	ITO/NiO_x/Me-4PACz/$(FA_{0.98}MA_{0.02})_{0.95}Cs_{0.05}Pb(I_{0.98}Br_{0.02})_3$/PEABr/PCBM+$C_{60}$/BCP/Ag	25.09	NO	2023	[50]
	ITO/NiO_x/TBT-BA/$Cs_{0.04}(FA_{0.96}MA_{0.04})_{0.96}Pb(I_{0.96}Br_{0.04})_3$/PCBM/BCP/Ag	24.80	NO	2024	[51]
	FTO/NiO_x/4PACz/$Cs_{0.05}MA_{0.05}FA_{0.90}PbI_3$/$C_{60}$/BCP/Ag	26.40	NO	2023	[52]
	ITO/NiO_x/Me-4PACz/$Cs_{0.05}FA_{0.85}MA_{0.1}PbI_3$/PDAI/$C_{60}$/BCP/Ag	**25.73**	**22.54**	**This work**	

[#] Corresponding abbreviation in the Architecture column of Table S4: 1-Benzyl-3-methylimidazolium bromide (BzMIMBr), poly[bis(4-phenyl) (2,4,6-trimethylphenyl) amine] (PTAA), 4-(3,6-dimethyl-9H-

carbazol-9-yl) butyl)-phosphonic acid (Me-4PACz), phenethylammonium bromide (PEABr), triphenylamine functionalized benzothiadiazole and benzoic acid (TBT-BA), [4,5-b'] dithiophene-3,9-diamine (DTD), piperazinium diiodide (PDI), fullerene (C60). * The citation numbers of the references in Table S4 are based on those in the full article.

Table S5. Summary of photovoltaic parameters for the devices based on different HTLs measured under standard AM 1.5 G illumination (100 mW cm^{-2}).

HTLs	V_{oc} (V)	J_{sc} (mA/cm^2)	FF (%)	PCE (%)
NiO$_x$	1.147	24.41	76.82	21.54
E-NiO$_x$	1.148	24.95	77.80	22.32
H-NiO$_x$	**1.168**	**25.23**	**83.56**	**24.69**
D-NiO$_x$	1.152	24.83	79.50	22.77

References

[1]   Z. Q. Huang, X. T. Hu, C. Liu, L. C. Tan, Y. W. Chen, *Adv. Funct. Mater.* **2017**, *27*, 1703061.

[2]   G. Kresse, J. Furthmüller, *Comput. Mater. Sci.* **1996**, *6*, 15-50.

[3]   G. Kresse, J. Furthmüller, *Phys. Rev. B* **1996**, *54*, 11169-11186.

[4]   J. P. Perdew, K. Burke, M. Ernzerhof, *Rev. Lett.* **1996**, *77*, 3865-3868.

[5]   G. Kresse, D. Joubert, *Phys. Rev. B* **1999**, *59*, 1758-1775.

[6]   P. E. Blöchl, *Phys. Rev. B* **1994**, *50*, 17953-17979.